AIAA JOURNAL
Vol. 41, No. 10, October 2003

Inverse Method for Identification of Acoustic Sources at Launch Vehicle Liftoff

Stephane Alestra* and Isabelle Terrasse†
European Aeronautic Defence and Space Company Corporate Research Center, 92150 Suresnes, France
and
Bernard Troclet‡
European Aeronautic Defence and Space Company Launch Vehicles, 78130 Les Mureaux, France

At liftoff, launch vehicles are subjected to a very severe overpressure and to an acoustic environment that can induce loads acting on payloads in the low-frequency domain (frequencies lower than 40 Hz). The overpressure starts at ignition of solid-rocket motors. This overpressure phase is followed by the acoustic phase. The liftoff acoustic environment is generated by the rocket exhausts and by their impingement on the launch pad. For a numerical prediction of the acoustic environment, the European Aeronautic Defence and Space Company has developed an inverse method via a time domain boundary integral equations approach that uses an optimal control method, with direct and adjoint equations. The corresponding discrete schemes are highly accurate and unconditionally stable. As an industrial application, the identification of acoustic sources is shown, on the liftoff acoustic environment of ARIANE 5. With the sources from acoustic pressure measurements on the upper part of the ARIANE 5 vehicle and on the pylons around the launch pad having been localized and characterized in the time domain, the complete environment is recovered. By integration of the resulting acoustic pressures over all surfaces of the launchers, the loads created by the liftoff acoustic field can be estimated.

Nomenclature

c	=	sound speed in the air
D	=	integral surface operator
F	=	set of source parameters
f_{p_l}	=	source label, equal to f, the parameter vector
f_p^j	=	source label equal to the p parameter component equal to the j of the vector
j	=	iteration
$j(F)$	=	cost function
K	=	number of sensors
k	=	label equal to the k of the sensor
$L()$	=	Lagrangian
N	=	number of solver time iterations
N_f	=	number of degrees of freedom on the obstacle boundary
N_s	=	number of sources
n	=	discrete current iteration
$O^e_{\text{diff}}(x, t)$	=	scattered field outside the obstacle
$O^i_{\text{diff}}(x, t)$	=	scattered field inside the obstacle
O^n_{diff}	=	exterior scattered field source equal to p; time n
$O^{n,p}_{\text{inc}}(f_p)$	=	incident field; source equal to p; time equal to n
$O_{\text{obs}}(x, t)$	=	measured observed pressure
O^n_{obs}	=	observed data time n
$O^p_{\text{inc}}(x, t)(f_p)$	=	incident field for source p
$O_{\text{tot}}(x, t, F)$	=	total field (outside)
O^d_{tot}	=	discrete direct total field
$O^{d^*}_{\text{tot}}$	=	discrete adjoint total field
O^n_{tot}	=	total field; source equal to p; time n
p	=	label equal to p of the source
Q^m	=	postprocess acoustic matrix time m
R^m	=	surface acoustic convolution matrix for time m
$S^n(f_p)$	=	boundary traces of the incident field source equal to p; time equal to n
$S^n_i(f_p)$	=	boundary traces of the incident field for source label equal to p; time equal to n; basis function equal to i
t	=	time variable
t_j	=	discrete time (real value) $j\Delta t$
U	=	acoustic pressure jump across the boundary
U^d	=	discrete direct boundary unknown
U^{d^*}	=	discrete adjoint boundary unknown
U^m	=	boundary acoustic unknown time m
x_k	=	location of sensor label equal to k
x, y	=	spatial variables in three dimensions
y_p	=	location of source label equal to p
Γ	=	obstacle boundary
γ_m	=	time basis function
Δt	=	time step
φ_i	=	spatial basis function
Ψ	=	test function (in variationnal formulation)
Ω^e	=	exterior domain obstacle
Ω^i	=	interior domain obstacle

Presented as Paper 2002-0926 at the AIAA 40th Aerospace Sciences Meeting, Reno, NV, 14–17 January 2002; received 7 December 2002; revision received 2 January 2003; accepted for publication 19 March 2003.

*Head, Inverse Problems Project, Mathematics for Modelling Department.
†Head, Mathematics for Modelling Department.
‡Head, Vibroacoustic and Fast Transient Analysis Department. Member AIAA.

I. Introduction

A. Industrial Problem

DURING the liftoff phase, launch vehicles, such as the ARIANE 5 launcher, are subjected to severe loads from overpressure and the acoustic environment. The overpressure loads and the acoustic loads are among the most severe loads that a launcher can encounter during flight. The initial cause of the two load cases is the rocket exhausts and their interactions with the launch pad (Figs. 1 and 2).

At rocket motor ignition, the sudden initiation of rocket exhausts in the launch duct has an effect similar to the upward motion of a piston, causing compression waves that propagate outside the launch duct and, consequently, excite the launcher. In the case of

Fig. 1 ARIANE 5 liftoff.

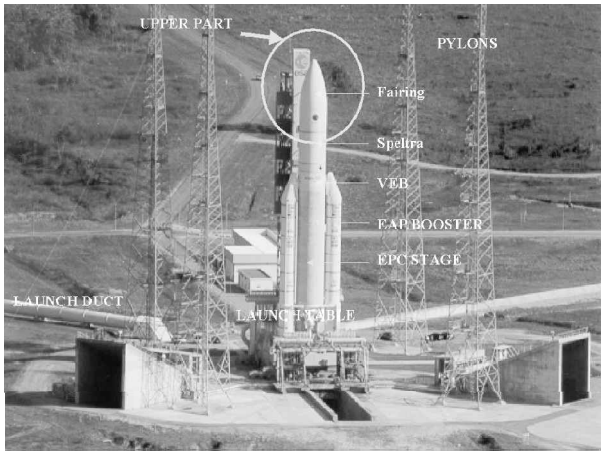

Fig. 2 ARIANE 5 on its launch pad.

ARIANE 5, the overpressure at motor ignition is generated by the EAP (etages d'accélération à poudre; solid-rocket booster) solid-rocket motors.

The overpressure is composed of the ignition overpressure (IOP), which originates from the launch table, and the duct overpressure (DOP), which originates from the launch ducts. Figures 2–4 illustrate this point with a picture of the ARIANE 5 launch pad, with the ducts.

The overpressure is a deterministic load having discrete spikes at particular frequencies, with significant levels for frequencies lower than 40 Hz. The primary sources of the acoustic field are the fluctuating turbulences in the mixing region of the rocket exhaust flow. The acoustic loads are random and broadband. This paper is focused on the low-frequency part of the acoustic excitation spectrum.

These two low-frequency excitations excite the launch vehicle and induce quasi-static loads (QSL) at the payload/launcher interface (Fig. 5), which the payload has to endure. Consequently, it is important to predict these loads before launches.[1,2] However, the main difficulties in doing this are the following:

1) The overpressure can be predicted by Navier–Stokes codes. On the other hand, at present, no numerical method is available for predicting noise generated by rocket exhausts of launchers lifting off from a launch pad. There are some relevant publications in this area, but they only deal with undeflected rocket exhaust noise.[3] Consequently, the estimation of the acoustic excitation requires measurements from sensors mounted on the launch vehicles.

2) The overpressure and the acoustic field at liftoff are of different natures: The overpressure is a deterministic phenomenon analyzed in the temporal domain, whereas the acoustic excitation has some random characteristics and is broadband. The acoustic excitation is usually defined in the frequency domain, and, consequently, the response of structures to this excitation is also analyzed in the frequency domain.

3) In fact, the separation, in the temporal domain, between the overpressure and the acoustic phenomenon can not be unambiguously defined.

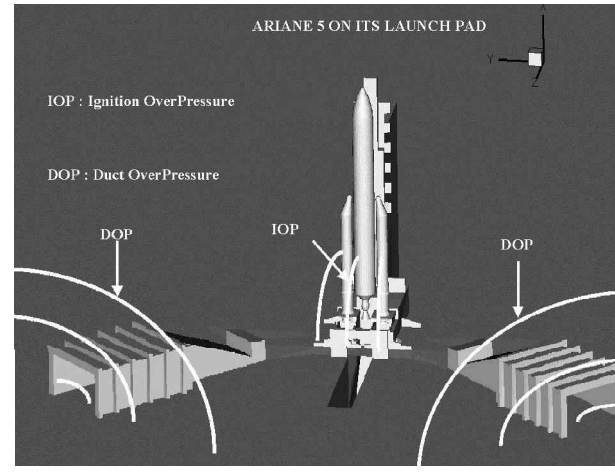

Fig. 3 IOP and DOP definition.

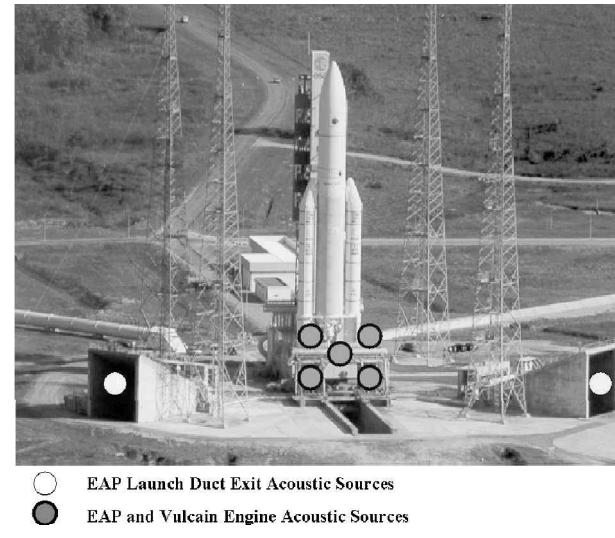

Fig. 4 Localization of ARIANE 5 low-frequency acoustic sources.

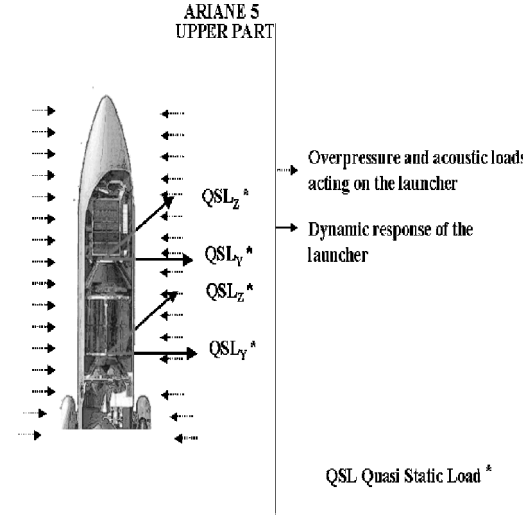

Fig. 5 Launch vehicle excitation cases at liftoff.

Thus, in view of these difficulties, it is not possible at the present time to specify an excitation defined in the time domain corresponding to the overpressure and acoustic phase for analyzing the low-frequency dynamic response of launchers during the complete liftoff phase. Currently, these two phases have to be distinguished: The dynamic response of vehicles and payloads to the overpressure is analyzed in the time domain, and the dynamic response to the acoustic excitation is studied in the frequency domain.

To avoid the aforementioned difficulties, our idea is to determine the acoustic sources from flight measurements in the temporal domain of both excitations (overpressure and acoustic excitations) by an inverse method. Now that the sources are localized, it will be easy to rebuild the unsteady pressure field and to estimate the pressure levels at any point on the vehicle. By the integration of the unsteady pressures over all surfaces of the launcher, the loads created by the liftoff acoustic field can be estimated. Consequently, the response of the launcher to these types of loads during the complete liftoff phase can be analyzed in the time domain with any finite element (FE) software.

Because, it seems, after preliminary investigations, that identification of the location of DOP and IOP sources (located at duct entrance and duct exit, respectively[4]) is easier than the identification of the acoustic sources, the work has begun with the identification of acoustic sources during the ARIANE 5 launch vehicle liftoff. This paper presents this work.

B. Introduction to the Inverse Acoustic Sources Problem

We have acoustic pressure measurements on the ARIANE 5 upper part and on the pylons, around the launch pad, on a discrete set of sensors associated with the ARIANE 503 flight. We denote the observed pressure by $O_{\text{obs}}(x_k, t_n)$. It is a function of the sensor number k, located at position x_k, and of discrete time n. In practice, k varies from 1 to $K = 14$ or $K = 23$ for the largest investigated example and n from 1 to $N = 300$ (number of time domain steps for one direct simulation), in most of our tests. Thus, we have a set of $300 \times 20 = 6000$ discrete data measurements points.

We wish to identify a set F of acoustic sources, parameterized by a real function f_p, which will be the control parameter variable used for the optimal control inverse method; f_p is associated with the pressure emitted by the source at point y_p:

$$F = \left(f_1, \ldots, f_p, \ldots, f_{N_s}\right) \tag{1}$$

In the time domain formulation used here, we assume that the emitter parameter function f_p also depends on the time evolution. For each time sampling j, we have the emission at source p, at time j:

$$f_p = \begin{bmatrix} f_p^1 = f_p(\Delta t) \\ \vdots \\ f_p^N = f_p(N\Delta t) \end{bmatrix} \tag{2}$$

The number of acoustic sources used varies from $N_s = 15$ to 20. Therefore, the method is said to be a multiparameter inverse acoustic sources problem because the number of parameters to be identified is $N_s \times N$ values, or approximately $15 \times 300 = 4500$ parameters.

We suppose that the associated incident acoustic source field O_{inc}^p emitted at the source p, depends on the parameter function f_p, as mentioned earlier:

$$O_{\text{inc}}^p(x, t)(f_p) = \frac{f_p(t - |x - y_p|/c)}{4\pi|x - y_p|} \tag{3}$$

The set F of all of these acoustic fields is radiated in the air, reflected by the launcher, producing the scattered field O_{diff}^e. The total computed field O_{tot} is the sum of this scattered and the direct incident fields:

$$O_{\text{tot}}(F) = O_{\text{tot}}(x, t, F) = O_{\text{diff}}^e(x, t) + \sum_{p=1}^{N_s} O_{\text{inc}}^p(x, t)(f_p) \tag{4}$$

This field O_{tot} can then be compared to the observed field O_{obs} at the points of observation x_k and at the discrete time t_n. The quadratic error or cost function $j(F)$, depending on the set F of source parameters, is defined by

$$j(F) = J[O_{\text{tot}}(F)] = \sum_{n=1}^{N} \sum_{k=1}^{K} (O_{\text{tot}} - O_{\text{obs}})^2(x_k, t_n, F) \tag{5}$$

The objective is to find a set of sources F that minimize the cost function $j(F)$.

We use a classical optimal control methodology[5] to build the gradients of $j(F)$ for variations in F. These techniques will be detailed in Sec. III. Section II is devoted to a description of the computation of the direct problem.

II. Direct Acoustic Problem

We consider the scattering problem of transient acoustic waves in a fluid medium by a submerged rigid object. Let Ω^i be a three-dimensional object with a regular (without tip) bounded surface $\Gamma = \partial\Omega^i$. Let $\Omega^e = R^3 \backslash \Omega^i$ denote the exterior domain occupied by the fluid medium. The domain Ω^e is assumed to be connected, but not Ω^i. We denote by O_{diff}^e the scattered acoustic pressure created in the fluid medium by an incident field O_{inc}^p (the wave propagating without the obstacle) and the contribution of a time domain point source number p. [See Eq. (3).]

Therefore, we have the following initial boundary value problem:

$$\begin{cases} \dfrac{1}{c^2}\dfrac{\partial O_{\text{diff}}^e(x,t)}{\partial t^2} - \Delta O_{\text{diff}}^e(x,t) = 0, & \text{in} \quad \Omega^e \times R^+ \\ O_{\text{diff}}^e(x,0) = \dfrac{\partial O_{\text{diff}}^e}{\partial t}(x,0) = 0, & \text{in} \quad \Omega^e \\ \dfrac{\partial O_{\text{diff}}^e}{\partial n} = -\displaystyle\sum_{p=1}^{N_s} \frac{\partial O_{\text{inc}}^p}{\partial n} & \text{on} \quad \Gamma \times R^+ \end{cases} \tag{6}$$

where n denotes the unit normal vector to Γ, oriented from domain Ω^I to $\Omega^{e,}$; c is the speed of sound in the medium. There are many methods to solve this problem by the use of boundary integral equations. Many authors have developed these methods in acoustics,[6,7] electromagnetism,[8,9] or elastodynamics.[10]

Some authors[11,12] have implemented variational approximation of time domain integral equations (TDIE) in acoustics and some others[13–15] have worked on the hybridization of TDIE with local partial differential equations (PDE).

Each method consists of looking for the solution as a prescribed combination of surface-retarded potentials and expressing the boundary condition as a function of the densities of the potentials. Equivalently, this corresponds to associating the exterior problem with an appropriate interior problem.

In this paper, we consider the following interior problem:

$$\begin{cases} \dfrac{1}{c^2}\dfrac{\partial O_{\text{diff}}^i(x,t)}{\partial t^2} - \Delta O_{\text{diff}}^i(x,t) = 0 & \text{in} \quad \Omega^i \times R^+ \\ O_{\text{diff}}^i(x,0) = \dfrac{\partial O_{\text{diff}}^i}{\partial t}(x,0) = 0 & \text{in} \quad \Omega^i \\ \dfrac{\partial O_{\text{diff}}^i}{\partial n} = -\displaystyle\sum_{p=1}^{N_s} \frac{\partial O_{\text{inc}}^p}{\partial n} & \text{on} \quad \Gamma \times R^+ \end{cases} \tag{7}$$

Now, let us denote by U the unknown function that is equal to O_{diff}^e in Ω^e and O_{diff}^i in Ω^i. It is well-known that, because O_{diff}^e is a solution of the wave equation (6) in $R^3 \backslash \Gamma$, it satisfies the following representation formula:

$$O_{\text{diff}}^e(x, t) = -\frac{1}{4\pi}\int_\Gamma n_y \cdot \nabla_x \frac{U(y, t - |x - y|/c)}{|x - y|}\,\mathrm{d}y$$

$$\forall x \in \Omega^i \cup \Omega^e \tag{8}$$

where

$$U = O^i_{\text{diff}} - O^e_{\text{diff}} \tag{9}$$

is the jump of O^e_{diff} crossing Γ, and $\tau = t - |x-y|$ is the retarded time. Using formula (8) to compute the traces of $O^e_{\text{diff}}\Gamma \times R^+$, as a function of U, and introducing the results in the boundary conditions of Eqs. (6) and (7), one obtains the following retarded potential boundary integral equations for the unknown function U:

$$DU(x,t) = \sum_{p=1}^{N_s} \frac{\partial O^p_{\text{inc}}}{\partial n}(x,t), \qquad \forall x \in \Gamma \tag{10}$$

with the surface operator D

$$DU(x,t) = -\lim_{x' \in \Omega^+ \to x} n_x \cdot \nabla_{x'} \left\{ \frac{1}{4\pi} \int_\Gamma n_y \cdot \nabla_{x'} \left[\frac{U(y, t-|x'-y|/c)}{|x'-y|} \right] d\sigma_y \right\} \tag{11}$$

Note that the operator D contains a hypersingular kernel and has to be defined properly. One can do this by a method of regularization. The main results are the existence and uniqueness of the solutions in some Sobolev space, as well as a priori estimates with respect to the data, and, finally, the property of finite velocity of propagation that implies that the solution at time t depends only on the data at times $s <= t$. A coerciveness property linked with an energy identity is available, facilitating the analysis of the approximation schemes.

An equivalent formulation of Eq. (10) is developed in Refs. 16–21. It can be written, with function U in $H^2[R+, H^{1/2}(\Gamma)]$, such that, for all Ψ in the same space

$$\int_{\Re} \int_{\Gamma\times\Gamma} \frac{\boldsymbol{n}(x)\boldsymbol{n}(y)}{4\pi|x-y|} \frac{\partial^2 U}{\partial t^2}\left(y, t - \frac{|x-y|}{c}\right) \frac{\partial \Psi}{\partial t}(x,t)\, dx\, dy\, dt + c^2 \int_{\Re} \int_{\Gamma\times\Gamma} \frac{\text{curl}_\Gamma U}{4\pi|x-y|}\left(y, t - \frac{|x-y|}{c}\right) \text{curl}_\Gamma \frac{\partial \Psi}{\partial t}(x,t) \times dx\, dy\, dt = \int_{\Re}\int_\Gamma \left(\sum_{p=1}^{N_s} \frac{\partial O^p_{\text{inc}}(x,t)}{\partial n} \right) \frac{\partial \Psi}{\partial t}(x,t)\, dx\, dt \tag{12}$$

Equation (12) is solved in space by a surface FE method. The boundary Γ of the object is meshed with N_h triangular elements. A $P1$ discretization in space and time is used. Each spatial basis function is associated with one vertex:

$$\varphi_i(S_j) = \delta_{ij}, \qquad \varphi_i \tag{13}$$

which represents the Kronecker symbol on each triangle. Time domain basis functions are denoted

$$\gamma_n(t) = \begin{cases} \dfrac{t - t_{n-1}}{\Delta t} & \text{if} \quad t \in [t_{n-1}, t_n] \\ -\dfrac{t - t_{n+1}}{\Delta t} & \text{if} \quad t \in [t_n, t_{n+1}] \\ 0 & \text{else} \end{cases} \tag{14}$$

After the discretization of Eq. (12), we obtain the following time-marching matrix system, denoting, by U^m, the solution vector (unknown acoustic pressure jump on the interface Γ, at time t^m)

$$\sum_{m=1}^{n} R^{n-m+1} U^m = \sum_{p=1}^{N_s} S^n(f_p) \tag{15}$$

solved at each time step, by inversion of the matrix R^1,

$$R^1 U^n = \sum_{p=1}^{N_s} S^n(f_p) - R^2 U^{n-1}, \ldots, -R^n U^1 \tag{16}$$

where U^m is a vector whose dimension is N_f, the number of degree of freedom on the obstacle; R^{n-m+1} an acoustic $N_f \times N_f$ matrix discussed in Ref. 2; and S^n, the N_f dimension vector, is the contribution of the incident fields on the interface Γ, at time t_n. Thus, we have,

$$U^m = \begin{bmatrix} U^m_1 \\ \vdots \\ U^m_{N_f} \end{bmatrix}, \qquad S^n(f_p) = \begin{bmatrix} S^n_1(f_p) \\ \vdots \\ S^n_{N_f}(f_p) \end{bmatrix} \tag{17}$$

with

$$S^n_i(f_p) = \int_{t_{n-1} \le t \le t_n} \int_\Gamma \frac{\partial O^p_{\text{inc}}(x,t)}{\partial n} \varphi_i(x)\, dx\, dt \tag{18}$$

Using an energy identity, we are able to prove the unconditional stability of this scheme. The method is described in some detail in Refs. 11 and 19–24, and its implementation has confirmed stability in a wide range of situations and for large run times never reached before. See also Refs. 25–27 for more comments on the stability question. Moreover, all of the acoustic matrices are real, sparse, and symmetric.

After the discretization of formula (8) in time and space, the computed scattered acoustic field is given by the forward marching time postprocess:

$$O^n_{\text{diff}} = \sum_{m=1}^{n} Q^{n-m+1} U^m \tag{19}$$

with

$$O^n_{\text{diff}} = \begin{bmatrix} O^n_{\text{diff}_1} \\ \vdots \\ O^n_{\text{diff}_K} \end{bmatrix} = \begin{bmatrix} O_{\text{diff}}(x_1, t_n) \\ \vdots \\ O_{\text{diff}}(x_K, t_n) \end{bmatrix} \tag{20}$$

and $Q^{n-m+1} K \times N_f$ postprocess rectangular matrices (operator from the interface Γ to near-field exterior points).

III. Inverse Acoustic Problem

As in Sec. II, we recall that the incident acoustic field is a point source emitter (from the point y_p), with control parameter variable p. From Eq. (3), we define the discrete incident field at the instant n, for the source p, observed at discrete points x_k (vector of dimension K):

$$O^{n,p}_{\text{inc}}(F) = \begin{bmatrix} \left(O^{n,p}_{\text{inc}}\right)_1 \\ \vdots \\ \left(O^{n,p}_{\text{inc}}\right)_K \end{bmatrix}(F)$$

with

$$\left(O^{n,p}_{\text{inc}}\right)_k(F) = \frac{f_p(t_n - |x_k - y_p|/c)}{4\pi|x_k - y_p|} \tag{21}$$

Using Eq. (4), we denote by

$$O^n_{\text{tot}} = O^n_{\text{diff}} + \sum_{p=1}^{N_s} O^{n,p}_{\text{inc}}(F) \tag{22}$$

with

$$O^n_{\text{tot}} = \begin{bmatrix} O^n_{\text{tot}_1} \\ \vdots \\ O^n_{\text{tot}_K} \end{bmatrix} = \begin{bmatrix} O_{\text{tot}}(x_1, t_n) \\ \vdots \\ O_{\text{tot}}(x_K, t_n) \end{bmatrix} \tag{23}$$

the total discrete computed (or synthetic) acoustic field data (summation of scattered and incident fields) at instant n, for the discrete points x_k. Denote by O^n_{obs} the discrete total observed (or measured acoustic field data) at instant n. The inverse problem is the identification of the vector parameter F, given the measured acoustic field O^n_{obs}.

We introduce the two discrete quantities

$$U^d = (U^1, \ldots, U^N), \qquad O^d_{\text{tot}}(F) = \left[O^1_{\text{tot}}(F), \ldots, O^N_{\text{tot}}(F)\right] \quad (24)$$

and the two following discrete scalar products:

$$(a^n, b^n)_{N_f} = \sum_{k=1}^{N_f} a^n_k b^n_k$$

for elements on the boundary such as U^n, of dimension N_f [see Eq. (17)]

$$(a^n, b^n)_K = \sum_{k=1}^{K} a^n_k b^n_k$$

for elements on the exterior domain, such as O^n_{tot}, of dimension K. [See Eq. (23).]

The discrete cost function, introduced in Eq. (5), is given by

$$j(F) = J\left[O^d_{\text{tot}}(F)\right] = \sum_{n=1}^{N} \left[O^n_{\text{tot}}(F) - O^n_{\text{obs}},\, O^n_{\text{tot}}(F) - O^n_{\text{obs}}\right]_K \quad (25)$$

The optimal source function $(f_p)_{\text{opt}}$ is given by

$$j(F_{\text{opt}}) = \min_F j(F) \quad (26)$$

under the two discretized constrained equations, the first being the discretized integral equation (15) and the second the discretized postprocessus equation (19).

By introduction of the following discrete adjoint variables or Lagrange multiplicator (see Refs. 5 and 18):

$$U^{d^*} = \left(U^{1^*}, \ldots, U^{N^*}\right) \qquad O^{d^*}_{\text{tot}} = \left(O^{1^*}_{\text{tot}}, \ldots, O^{N^*}_{\text{tot}}\right)$$

The classical Lagrangian formulation is obtained from

$$L\left(F, U^d, U^{d^*}, O^d_{\text{tot}}, O^{d^*}_{\text{tot}}\right) = J\left(O^d_{\text{tot}}\right) + \sum_{n=1}^{N} \left(U^{n^*}, \sum_{m=1}^{n} R^{n-m+1} U^m - \sum_{p=1}^{N_s} S^n(f_p) \right)_K + \sum_{n=1}^{N} \left(O^{n^*}_{\text{tot}}, O^n_{\text{tot}} - \sum_{m=1}^{n} Q^{n-m+1} U^m - \sum_{p=1}^{N_s} O^{n,p}_{\text{inc}}(f_p) \right)_{N_f} \quad (27)$$

We know that if $(F, U^d, U^{d^*}, O^d_{\text{tot}}, O^{d^*}_{\text{tot}})$ is a saddle point of the Lagrangian, then F is at least a local minimum of the constrained cost function.

The optimality conditions corresponding for U^{d^*} and $O^{d^*}_{\text{tot}}$ are equivalent to the direct problem (15) and (19). The optimality conditions written for U^d and O^d_{tot} are

$$\frac{\partial L}{\partial U^m}\left(F, U^d, U^{d^*}, O^d_{\text{tot}}, O^{d^*}_{\text{tot}}\right) = 0, \qquad \forall m \in [1, N] \quad (28)$$

$$\frac{\partial L}{\partial O^m_{\text{tot}}}\left(F, U^d, U^{d^*}, O^d_{\text{tot}}, O^{d^*}_{\text{tot}}\right) = 0, \qquad \forall m \in [1, N] \quad (29)$$

These conditions give the two following steps for discretization of a time backward adjoint system:

$$O^{N^*}_{\text{tot}} = \sum_{k=1}^{K} \left(O^N_{\text{tot}} - O^N_{\text{obs}}\right)$$
$$\vdots$$
$$O^{1^*}_{\text{tot}} = \sum_{k=1}^{K} \left(O^1_{\text{tot}} - O^1_{\text{obs}}\right) \quad (30a)$$
$$(R^1)^* U^{N^*} = -Q^{N^*} O^{N^*}_{\text{tot}}$$
$$(R^1)^* U^{1^*} + \cdots + (R^N)^* U^{N^*} = -\sum_{n=1}^{N} Q^{n^*} O^{n^*}_{\text{tot}} \quad (30b)$$

Note that the time evolution system direct (forward) and adjoint (backward) codes have exactly the same properties. Therefore, the adjoint scheme is also unconditionally stable.

The gradient formulas for $j(F)$ for changes in F are then derived, for the parameter function f_p:

$$\frac{\partial j}{\partial f_p} = \frac{\partial L}{\partial f_p} = -\sum_{n=1}^{N} \left\langle U^{n^*}, \frac{\partial S^n(f_p)}{\partial f_p} \right\rangle - \sum_{n=1}^{N} \left\langle O^{n^*}_{\text{tot}}, \frac{\partial O^{n,p}_{\text{inc}}}{\partial f_p} \right\rangle \quad (31)$$

and have to be written for each time iteration j, for the two variables $T = S^n$ and $T = O^{n,p}_{\text{inc}}$, with

$$f_p = \left(f^1_p, \ldots, f^N_p\right) \qquad \frac{\partial T}{\partial f_p} = \left(\frac{\partial T}{\partial f^1_p}, \ldots, \frac{\partial T}{\partial f^N_p}\right)$$

We need to compute

$$\frac{\partial\left(S^n_i\right)}{\partial f^j_p}, \qquad \frac{\partial\left(O^{n,p}_{\text{inc}}\right)_k}{\partial f^j_p}$$

in Eq. (31). The incident field (21) is approximated in time and, by the use of the $P1$ space basis functions γ^j, Eq. (14), we denote

$$\left(O^{n,p}_{\text{inc}}\right)_k(F) = \frac{f_p(t_n - |x_k - y_p|/c)}{4\pi|x_k - y_p|} = \frac{\sum_{j=1}^{N} f^j_p \gamma_j(t_n - |x_k - y_p|/c)}{4\pi|x_k - y_p|} \quad (32)$$

The discretized right-hand side S^m of Eq. (18) is then written (for the ith spatial basis function)

$$S^n_i(f_p) = \int_{t_{n-1} \le t \le t_n} \int_{\Gamma} \frac{\partial O^p_{\text{inc}}(x,t)}{\partial n} \varphi_i(x)\, \mathrm{d}x\, \mathrm{d}t = \sum_{j=1}^{N} f^j_p A^{n,j}_{p,i} \quad (33)$$

With the discrete matrix $A^{n,j}_{p,i}$ given in Ref. 21.

Therefore,

$$\frac{\partial S^n_i}{\partial f^j_p} = A^{n,j}_{p,i} \quad (34)$$

From Eq. (32), the computation of $\partial O^{n,p}_{\text{inc}}/\partial f_p$ gives

$$\left[\frac{\partial\left(O^{n,p}_{\text{inc}}\right)_k}{\partial f^j_p}\right] = \frac{\gamma_j(t_n - |x_k - y_p|/c)}{4\pi|x_k - y_p|} \quad (35)$$

The expression of the gradients (31) is now completely established. With an initial guess for the estimated parameter f^0_p, a quasi-Newton optimizer is used to update the parameter value f^n_p at the optimizer step l and to find the optimal f_p that causes the gradients to vanish. L is the number of optimizer steps at the end of the inverse process:

$$\left(f^j_p\right)^{l+1} = \left(f^j_p\right)^l - \left[H^{-1}(\partial j/\partial f_p)\right]^l_j \quad (36)$$

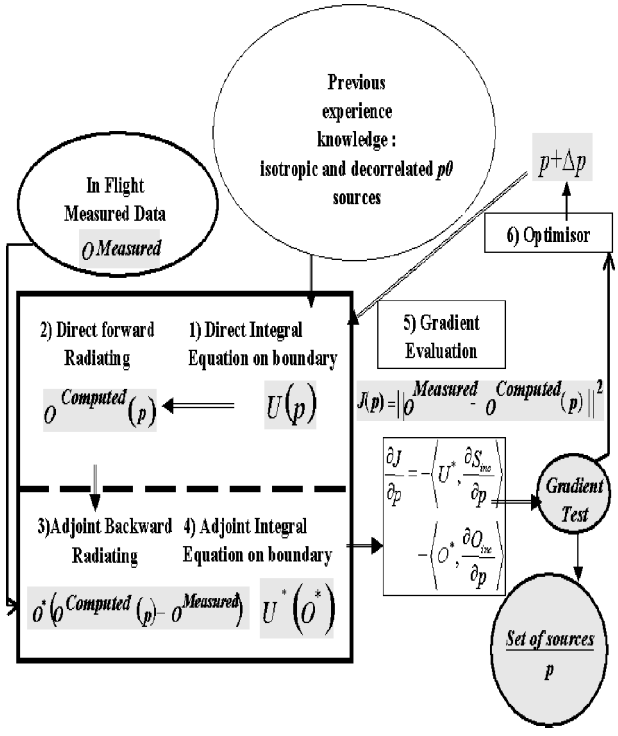

Fig. 6 Global scheme of the inverse process minimization loop.

with H^{-1} a positive-definite matrix that approximates the inverse of the Hessian of the cost function. The gradient value is computed by formula (31), for the optimizer step l. A global view of the minimization process is shown Fig. 6.

IV. Numerical Applications: ARIANE 503 Flight Inverse Acoustic Source Problem

The methodology has been validated on the ARIANE 5 third and fourth flights. The analysis was performed in the time period when the acoustic environment was at its maximum.

An acoustic antenna having 14 acoustic measurements points has been mounted on the upper part of ARIANE 5, and some other acoustic measurement have been installed on four pylons around the launch pad.

A surface mesh of ARIANE 5 has been made using the SDRC IDEAS software and is approximately composed of 1000 triangular surface elements. The inverse acoustic analysis has to cover the low-frequency range 0/40 Hz (measurement data are consequently filtered). The size of a typical element is around $\frac{1}{5}$ of the minimal acoustic wavelength of the time domain pulse, giving an element size of around 1.5 m.

Given the data measurement acquired during the 503 flight, two sets of sources (numerical test 1 and numerical test 2) are searched. The purpose is to define: 1) a finite number, as small as possible, of acoustic source locations and 2) acoustic sources, as simple as possible, to investigate if it is possible to restore the acoustic levels measured on the launcher with sufficient precision (within 20%) with simple sources. We have chosen isotropic sources. Given our experience, we had an idea of the acoustic source locations[28,29]: below the launcher and at the launch duct exit. The influence of the number of sources has been analyzed with the two numerical tests explained now.

A. Numerical Test 1 Definition

There are 14 sensors ($K = 14$) on the upper part of the launcher (fairing, speltra, vehicle equipment bay, etc.). There are seven acoustic sources ($N_s = 7$): one source located at each duct exit, two acoustic sources under each EAP (etage principal cryothechnique;central engine stage) solid-rocket booster and one source under the EPC Vulcain engine. The initial guess for the seven sources is chosen to equal zero.

B. Numerical Test 2 Definition

There are 14 sensors ($K = 14$) on the upper part of the launcher (fairing, speltra, vehicle equipment bay, etc.). There are 11 acoustic sources ($N_s = 11$): three acoustic sources on each duct exit, two acoustic sources under each EAP solid-rocketbooster, and one under the EPC Vulcain engine. The initial guess for the 11 sources is chosen to equal zero.

Localization of sources 1–7 is the same for numerical test 1 and numerical test 2. Compared to numerical test 1, the number of acoustic sources in numerical test 2 is increased. For the two cases, one direct code simulation requires $N = 250$ time steps, with a time step of $\Delta t = 4.5e - 3$ s. On a Unix workstation, two days computation are necessary for the whole inversion process ($L = 350$ optimizer step iterations).

Recall that the quadratic error or cost function $j(F)$, depending on the set F of source parameters, is the quadratic error between measurements data O_{obs} and computed data O_{tot}. [See Eq. (3).]

Some of the common (Figs. 7–9, sources 1/3/5) and some of the additional (Fig. 10, source 8) physical sources from numerical

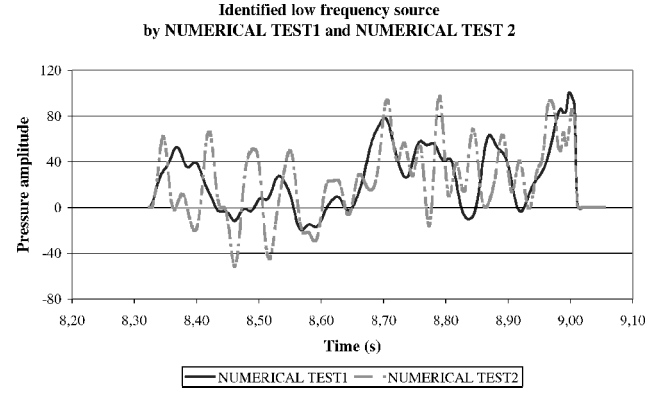

Fig. 7 Acoustic source 1 (left launch duct exit).

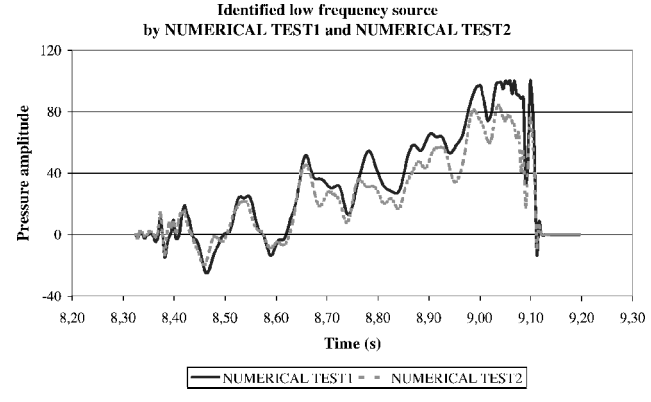

Fig. 8 Acoustic source 3 (right solid-rocket booster).

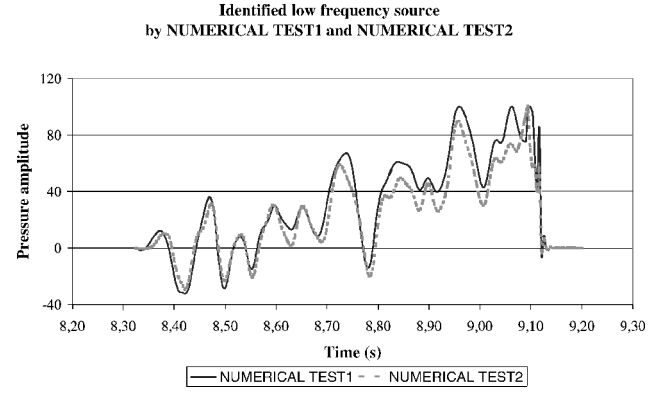

Fig. 9 Acoustic source 5 (Vulcain central engine).

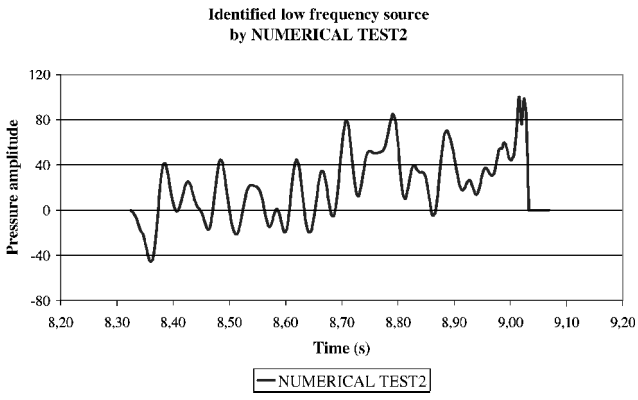

Fig. 10 Acoustic source 8 (left launch duct exit 2).

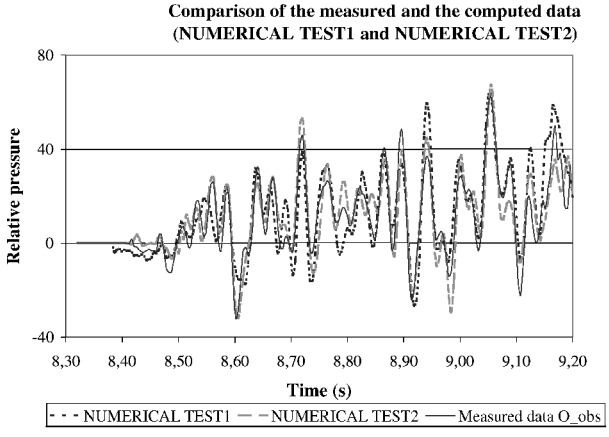

Fig. 11 Comparison of the measured and computed data (sensor 1, vehicle equipment bay).

test 1 and numerical test 2, obtained after the inversion process, are displayed. The source evolution f_p in the time domain (relative amplitude) is plotted, for each time step $j < N = 250$ of the time observation interval 8.3/9.1 s (with a numerical truncation at 9.1 s). We see few differences in the evolution vs time of common physical sources, when the number of sources is increased ($K = 7$ and 11).

We find by the calculations the asymmetry of the left and right launch ducts and of the water injection positions in the launch ducts. Now, after identification of the acoustic source locations, a direct problem is solved in the two cases, to compute the acoustic levels at the locations where the 14 sensors are mounted on the upper part of the launcher. Those simulated acoustic levels are compared with the real measured values on the same sensors.

Some of the these sensors have been selected, and the comparisons for numerical test 1 and numerical test 2 between simulated acoustic pressures and measured data are plotted in Figs. 11 and 12. The agreement is quite good for the two cases. For all of the sensors, global error between simulated and measured data is no more than 10%, which is very small and, of course, lower than the margins taken into account in the estimation of limit loads. Although the sources are different, the simulated data from numerical test 1 and numerical test 2 are quite comparable, which shows the nonuniqueness of the inverse problem. We have also tested the stability of the inverse procedure for numerical test 1 identification.

We find that 10% noise on measurement data implies about 5% error on the identified sources and 20% error on simulated data in the launcher part. This error is lower than the margins taken into account in the estimation of limit loads. A Tichonov regularization process should be used to stabilize data errors and to compensate the ill-posed nature of inverse problems. This is explained in the literature, but, in our applications, the large dimension of parameter space might explain why our numerical inverse problem seems well posed.

Errors in direct simulation after identification are more important on the lower part than on the upper part because most of the sensor information comes from the upper part. To overcome this problem

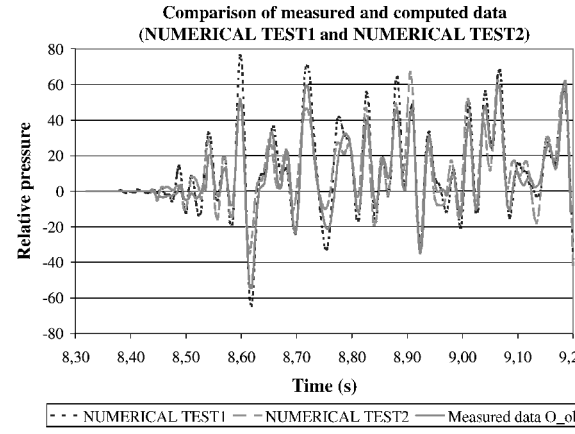

Fig. 12 Comparison of the measured and computed data (sensor 7, fairing).

of finding the true solution among many incorrect solutions (due to nonuniqueness), it might be useful to have a set of ground sensors, or to have a set of sensors mounted on the lower part of the launcher. A study to find optimal and efficient ground sensors, containing enough information to rebuild most of the acoustic environment on the upper part of the launcher, is under investigation.

V. Conclusions

A robust and accurate time domain integral equation for wave propagation was developed. The time-marching scheme for the direct acoustic source problem is unconditionally stable (no Courant–Friedrich–Lewy conditions). This allows a classical optimization approach for the inverse problem.

Direct and adjoint codes have exactly the same properties. Earlier knowledge of the localization of sources and power parallel computers allow the industrial application of such an inverse problem.

We demonstrate the method on some examples of source reconstructions in low-frequency acoustics for the ARIANE 5 acoustic source identification on the data from 503 ARIANE 5 flight: Initial results are very promising and show a good identification of the multiparameter sources in the 0–40 Hz frequency domain (source function at each time step), with partial acoustic data (launcher upper part sensors). Isotropic sources are sufficient to restore the acoustic levels measured on the launcher, with deviations no higher than 20%.

The acoustic loads due to supersonic jets are broadband. High-frequency acoustic loads encountered at launcher liftoff are random. However, acoustic levels for frequencies lower than 30/40 Hz are mainly due to deterministic phenomena. Indeed, from analysis of flight measurement, it appears that significant low-frequency acoustic levels are related to the geometrical dimensions of the launch pad. This is one reason for this success. The work was facilitated by the earlier knowledge of the acoustic source location. We have also shown the nonuniqueness of these inverse acoustic sources, which confirms that it might be difficult to simulate acoustic fields correctly in the launch pad ground zone, without sensors in this zone. However, a completely instrumented flight (both the upper part and the lower part of the ARIANE 5 launcher) is foreseen, to fix the source locations.

Future studies will be dedicated to the overpressure problem, and exploitation of the 504 ARIANE 5 flight is under way with regards to this problem. With regard to the locations of overpressure sources, it is assumed in most papers that they are on the launch table and at launch duct exit. According to those papers, like a space shuttle solid-rocket motor ignition overpressure prediction methodology, the propagation of IOP and DOP from the sources located on the launch pad to the launch vehicle can be predicted by linear acoustics. Consequently, for the overpressure sources localization studies, we will assume at first that the linear acoustics are valid, and we will check this hypothesis.

The ultimate goal is to define, in the temporal domain, the source of both phenomena occurring at liftoff: the overpressure and the

acoustic excitation. Once this is done, the complete pressure field applied to the launcher could be rebuilt.

Acknowledgments

This work was carried out at the European Aeronautic Defence and Space Co. (EADS) Corporate Research Center (CRC) and was supported by EADS Launch Vehicles, Les Mureaux, and the Centre National d'Etudes Spatiales, France. We would like also to thank Michèle Depuydt, Engineer at the Vibroacoustic and Fast Transient Analysis Department at EADS Launch Vehicles, Les Mureaux, for her participation in measurement data exploitation; François Dubois, from the Conservatoire National des Arts et Métiers (Paris) and Pierre-Louis Lions from Université PARIS IX (Paris) and l'Ecole Polytechnique (Palaiseau), for their contacts in the aerospace industry and academic scientific computing world; Eric Duceau, Head of the Scientific Environment Department at EADS CRC, for his support and anticipation on potential applications of inverse methods at EADS/CRC Suresnes; and Bruno Ludwig, whose Ph.D. dissertation addressed this subject at EADS CRC Suresnes.

References

[1]Troclet, B., Chemoul, B., Roux, P., Gely, D., and Elias, G., "Synthesis of Vibroacoustic Studies Performed During ARIANE 5 Program," *Launch Vehicle Vibrations*, Centre National d'Etudes Spatiales, Toulouse, France, 1999, pp. 201, 210.

[2]Troclet, B., Depuydt, M., and Rohne, P. B., "Experimental Analysis of Aerodynamic Noise on the Launch Vehicle Upper Part," AIAA 16th Aeroacoustics Conf., Munich, June 1995.

[3]Ding, Y., Forestier, A., and Ha-Duong, T., "A Galerkin Scheme for the Time Domain Integral Equation," *Journal of the Acoustical Society of America*, Vol. 86, No. 4, 1989, pp. 1566–1572.

[4]Ikawa, H., and Laspesa, F. S., "Ignition/Duct Overpressure Induced by Space Shuttle Solid Rocket Motor Ignition," *Journal of Spacecraft*, Vol. 22, No. 4, 1985, pp. 481–488.

[5]Lions, J. L., *Contrôle Optimal des Systèmes gouvernés par des Équations aux Dérivées Partielles*, Dunod, Paris, 1968.

[6]Ha Duong, T., "Equations Intégrales pour la Résolution Numérique des Problèmes de Diffraction d'Ondes Acoustiques," Ph.D. Dissertation, Université Paris VI, Paris, Sept. 1987.

[7]Hamdi, M. A., "Une Formulation Variationnelle par les Équations Intégrales pour la Résolution de l'Équation de Helmholtz avec des Conditions aux Limites Mixtes," *Comptes Rendus à l'Académie des Sciences, Série II*, Vol. 292, 1981, pp. 17–20.

[8]Bamberger, A., Chavent, G., and Lailly, P., "About the Stability of the Inverse Problem in 1D Wave Equation," *Journal of Applied Mathematics and Optimisation*, Vol. 5, 1979, pp. 1–47.

[9]Lange, V., "Equations Intégrales Espace-Temps pour les Équations de Maxwell. Calcul du Champ Diffracté par un Obstacle Dissipatif," Ph.D. Dissertation, Dept. of Applied Mathematics, Université Bordeaux I, Bordeaux, France, Sept. 1995.

[10]Becache, E., and Ha-Duong, T., "A Space–Time Variational Formula for the Boundary Integral Equation in a 2D Elastic Crack Problem," *Journal of Mathematics Modelling and Numerical Analysis*, Vol. 28, No. 2, 1994, pp. 141–176.

[11]Bachelot, A., and Pujols, A., "Equations Intégrales Espace-Temps pour le Système de Maxwell, *Comptes Rendus à l'Académie des Sciences, Série I*, t.314, 1992, pp. 639–644.

[12]Pujols, A., "Equations Intégrales Espace-Temps pour le Système de Maxwell. Application au Calcul de la Surface Équivalente Radar," Ph.D. Dissertation, Dept. of Applied Mathematics, Université de Bordeaux I, Bordeaux, France, Nov. 1991.

[13]Bluck, M. J., and Walker, S. P., "Time-Domain BIE Analysis of Large Three-Dimensional Electromagnetic Scattering Problems," *IEEE Transactions on Antennas and Propagation*, Vol. 45, No. 5, 1997, pp. 894–901.

[14]Dodson, S. J., Walker, S. P., and Bluck, M. J., "Implicitness and Stability of Time Domain Integral Equation Scattering Analyses," *ACES Journal*, Vol. 13, No. 3, 1998, pp. 291–301.

[15]Gres, N. T., Ergin, A. A, Shanker, B., and Michielssen, E., "Integral Equation Based Analysis of Transient Electromagnetic Scattering from Three Dimensional Inhomogeneous Dielectric Objects," *Proceedings of the 16th Annual Review of Progress in Applied Computational Electromagnetics*, Applied Computational Electromagnetics Society, Monterey, CA, 2000, pp. 647–653.

[16]Abboud, T., El Gharib, J., and Zhou, B., "Retarded Potentials for Acoustic Impedance Problems," *Proceedings of the 5th International Conference on Mathematical and Numerical Aspects of Waves Propagation*, Society for Industrial and Applied Mathematics, 2000, pp. 703–707.

[17]Abboud, T., and Sayah, T., "Retarded Potential Method for Computational Electromagnetics," *Proceedings of AP2000 Millennium Conference on Antennas and Propagation*, ESA, 2000.

[18]Alestra, S., "Méthodes Inverses en Électromagnétisme pour des Milieux Stratifiés, Bipériodiques et Bidimensionnels," Ph.D. Dissertation, Dept. of Mathematics, Université Paris XIII, Villetaneuse, France, July 1997.

[19]Terrasse, I., "Résolution Mathématique et Numérique des Équations de Maxwell Instationnaires par une Méthode de Potentiels Retardés," Ph.D. Dissertation, Dept. of Mathematics, Ecole Polytechnique, Palaiseau, France, Jan. 1993.

[20]Terrasse, I., "Résolution des Équations de Maxwell Instationnaires par une Méthode de Potentiels Retardés," *Proceedings of European Symposium on Numerical Methods in Electromagnetics JEE'93*, 1993, pp. 135–141.

[21]Terrasse, I., Ludwig, B., Alestra, S., Duceau, E., and Ha Duong, T., "Inverse Acoustic Impedance Problem Using the Delayed Time-Domain Boundary Integral Method," *Proceedings of the 5th International Conference on Mathematical and Numerical Aspects of Waves Propagation*, Society for Industrial and Applied Mathematics, 2000, pp. 667–671.

[22]Ludwig, B., "Etude de Quelques Problèmes Directs et Inverses en Propagation d'Ondes Acoustiques Transitoires. Méthodes d'Eléments Finis de Frontière," Ph.D. Dissertation, Dept. of Mathematics, Université de Compiègne, Compiègne, France, Nov. 2000.

[23]Alestra, S., Terrasse, I., Ludwig, B., and Duceau, E., "Inverse Electromagnetic Impedance Problem Using the Delayed Time-Domain Boundary Integral Method," *Proceedings of AP2000 Millennium Conference on Antennas and Propagation*, ESA, 2000.

[24]Filipe, M., Forestier, A., and Ha-Duong, T., "A Time Dependent Acoustic Scattering Problem," *Proceedings of the 3rd International Conference on Mathematics and Numerical Aspects of Wave Propagation Phenomena*, Mandelieu, 1995, pp. 140–150.

[25]Rao, S. M., and Sarkar, T. K., "Transient Analysis of Electromagnetic Scattering from Wire Structures Utilizing an Implicit Time-Domain Integral-Equation Technique," *Microwave and Optical Technology Letters*, Vol. 17, No. 1, 1998, pp. 66–69.

[26]Rynne, B. P., "Stability and Convergence of Time Marching Methods in Scattering Problems," *IMA Journal of Applied Mathematics*, Vol. 35, 1985, pp. 297–310.

[27]Vechinski, D. A., and Rao, S. M., "A Stable Procedure to Calculate the Transient Scattering by Conducting Surfaces of Arbitrary Shape," *IEEE Transactions on Antennas and Propagation*, Vol. 40, No. 6, 1992, pp. 661–665.

[28]Ikawa, H., and Laspesa, F. S., "Space Shuttle SRM Ignition Overpressure Prediction Methodology," *JANNAF 13th Plume Technology Meeting*, Chemical Propulsion Information Agency, CPIA Publ. 357, 1982, Laurel, MD, pp. 245–256.

[29]Freund, J. B., Lele, S. K., and Moin, P., "Numerical Simulation of a Mach 1.92 Turbulent Jet and Its Sound Field," *AIAA Journal*, Vol. 38, No. 11, 2000, pp. 2023–2031.

W. J. Devenport
Associate Editor